Catalysis Today 138 (2008) 175–182

Contents lists available at ScienceDirect

Catalysis Today

journal homepage: www.elsevier.com/locate/cattod

Hydrogen production by steam reforming of methanol over Cu–CeZrYO$_x$-based catalysts

P. Yaseneva [a], S. Pavlova [a,*], V. Sadykov [a], E. Moroz [a], E. Burgina [a], L. Dovlitova [a], V. Rogov [a], S. Badmaev [a], S. Belochapkin [b], J. Ross [c]

[a] Boreskov Institute of Catalysis, Pr. Lavrentieva 5, 630090, Novosibirsk, Russia
[b] Materials and Surface Science Institute, Limerick, Ireland
[c] University of Limerick, Ireland

ARTICLE INFO

Article history:
Available online 31 July 2008

Keywords:
Hydrogen production
Methanol steam reforming
Cu–Ce–Zr–Y mixed oxide catalysts
Alumina and chromium additives
Urea–nitrate combustion synthesis

ABSTRACT

Active and selective $Cu_x(CeZrY)_{1-x}O_y$ catalysts (pure and with addition of Al_2O_3 and Cr) for the steam reforming of methanol were synthesized via the urea–nitrate combustion method. Structural, surface and redox characteristics of these catalysts were investigated by XRD, BET, IR spectroscopy, differential dissolution (DD), H_2-TPR and XPS methods. It was shown that addition of alumina and Cr leads to the steep increase in H_2 production due to appearance of highly dispersed copper species and stabilizes their activity. The parallel change of SRM rate constants and maximal rates of reduction with hydrogen characterizing mobility of lattice oxygen at variation of the catalyst composition was revealed that shows the importance of lattice oxygen mobility for steam reforming of methanol.

1. Introduction

Steam reforming of methanol (SRM) is a promising route to produce hydrogen for proton-exchange membrane (PEM) fuel cells which can be an attractive power source for on-board or portable devices [1–4]. However, the development of productive and compact methanol processor demands to solve several challenges originating from the peculiarities of both the SRM, and the PEM fuel cells. A considerable amount (>100 ppm) of CO, which is a poison for Pt electrode in PEM fuel cells, is known to be produced during SRM, and a CO clean-up step of hydrogen prior to the fuel cell is required [2–4]. Present technology involves multi-step fuel processors with a sequence of SRM and water gas shift reaction. To reduce the CO content to ppm level in a compact processor, an attractive alternative could be a membrane reactor, which combines hydrogen permeable Pd-membranes with a methanol steam reformer. Such reactors effectively work at temperatures 270–350 °C [5,6] and SRM catalysts with a high-thermal stability are required.

Cu-containing catalysts are well known as the most active for steam reforming of methanol [2–9]. However, traditional CuO/ZnO or CuO/ZnO/Al_2O_3 catalysts have a low thermal and long-term stability at temperature near and above 300 °C. Therefore, the development of stable catalysts with a high selectivity and activity is desired. It was recently found that the catalysts based on Cu/CeO_2 possess good performance in reforming of methanol due to a high oxygen storage capacity of CeO_2 and a high oxygen mobility in its lattice which provide a fast transfer of bulk oxygen to the surface [10–13]. The activity of the catalysts can be adjusted by the addition of different cations such as Zr^{4+}, Y^{3+}, La^{3+}, Sm^{3+}, etc. [14–18]. The incorporation of triple-charged ions into the lattice of CeO_2 facilitates the diffusion of lattice oxygen due to formation of vacancies in the anion sublattice and decreases the temperature at which redox processes occur. On the other hand, addition of chromium and alumina increases a high catalyst surface area and its stability to sintering [19–21]. However, there are some contradicting data on the effect of CeO_2 dopant on the SRM activity of the catalysts. This could be due to the different methods of catalyst preparation and different concentrations of copper in the catalysts. Thus, for CuO–CeO_2 catalysts prepared by urea–nitrate combustion method, doping with small amounts of Sm and Zn has been shown to improve SRM activity, while addition of La, Zr, Mg, Gd, Y, Ca has a negligible effect, or even lowers the catalytic activity [15]. For the CuO–CeO_2 catalysts prepared by co-precipitation and containing 80 wt.% of CuO, the addition of ZrO_2, Al_2O_3 and Y_2O_3 was found to enhance their activity in SRM [16].

In the present work the catalysts based on Cu–Ce–Zr–Y mixed oxides (pure and with alumina and chromium additives) were synthesized using the urea–nitrate combustion method [13] and

* Corresponding author.
E-mail address: pavlova@catalysis.nsk.su (S. Pavlova).

0920-5861/$ – see front matter © 2008 Elsevier B.V. All rights reserved.
doi:10.1016/j.cattod.2008.06.012

Table 1
Encoding, composition, BET and XRD characteristics of the catalysts

Catalyst encoding	Composition	Cu Content (wt.%)	Surface area ($m^2\ g^{-1}$)	Lattice parameter, Å	Crystallite size (nm)
	CeO_2	–	33	5.416	9
$Cu_{0.15}C$	$Cu_{0.15}Ce_{0.85}O_y$	6	28	5.402	12
$Cu_{0.15}CZ$	$Cu_{0.15}Ce_{0.55}Zr_{0.3}O_y$	6.3	72	5.391	10
CZY	$Ce_{0.6}Y_{0.2}Zr_{0.2}O_y$	–	5	5.341	39
$Cu_{0.1}CZY$	$Cu_{0.1}Ce_{0.6}Zr_{0.1}Y_{0.2}O_y$	3.9	8	5.358	25; 10[a]
$Cu_{0.15}CZY$	$Cu_{0.15}\ Ce_{0.55}Zr_{0.1}Y_{0.2}O_y$	5.5	5	5.371	28; 15[a]
$Cu_{0.2}CZY$	$Cu_{0.2}\ Ce_{0.5}Zr_{0.1}Y_{0.2}O_y$	8.3	33	5.365	16; 19[a]
$Cu_{0.2}CZY10A$	$Cu_{0.2}Ce_{0.5}Y_{0.2}Zr_{0.1}O_y$ + 10% Al_2O_3	7.2	28	5.360	16; 5[a]
$Cu_{0.2}CZY20A$	$Cu_{0.2}Ce_{0.5}Y_{0.2}Zr_{0.1}O_y$ + 20% Al_2O_3	7.4	42	5.374	8.5
$Cu_{0.2}CZY40A$	$Cu_{0.2}Ce_{0.5}Y_{0.2}Zr_{0.1}O_y$ + 40% Al_2O_3	5.9	140	5.393	6.3
$Cu_{0.2}CZYCr40A$	$Cu_{0.2}Cr_{0.1}Ce_{0.5}Y_{0.1}Zr_{0.1}O_y$ + 40% Al_2O_3	7.4	165	5.371	4.5
$Cu_{0.3}CZYCr40A$	$Cu_{0.3}Cr_{0.1}Ce_{0.4}Y_{0.1}Zr_{0.1}O_y$ + 40% Al_2O_3	11.7	170	5.382	4.5

[a] Crystallite size of CuO.

influence of the chemical composition of the catalysts on their activity and stability in steam reforming of methanol was investigated. These results were analyzed with a due regard for the real structure of the catalysts, their surface composition and oxygen mobility/reactivity.

2. Experimental

2.1. Catalyst preparation and characterization

Two series of the catalysts were synthesized via the urea–nitrate combustion method [13,15]. The first was $Cu_{0.15}CeO_z$, $Cu_{0.15}Ce_{0.55}Zr_{0.3}O_z$, $Ce_{0.6}Y_{0.2}Zr_{0.2}O_z$ and mixed oxides of the general formula $Cu_xCe_{0.7-x}Y_{0.2}Zr_{0.1}$ (Cu_xCZY), where $x = 0.1–0.2$. In the second series, the samples with alumina and chromium additives were prepared. The composition of these catalysts corresponds to the formula $Cu_{0.2}(CeZrYCr)_{0.8}O_zyAl_2O_3$ ($Cu_{0.2}CZY(Cr)yA$), where 0.2 is an atomic ratio Cu/(Cu + Ce + Zr + Y + Cr) and $y = 10, 20, 40$ is the weight content of Al_2O_3. The composition and some characteristics of the samples are given in Table 1. For the catalysts preparation, the water solution of Cu, Ce, Zr, Y, Cr nitrates in the appropriate molar ratios was mixed with 100% urea excess relative to nitrates. In the case of the samples with the alumina additive, the corresponding amount of the alumina powder was added to the solution. The resulted solution was steamed until formation of a viscous gel and then was placed in the furnace, pre-heated to 400 °C, where combustion reaction took place. The products were further calcined at 400 °C for 3 h in air.

The specific surface area was determined by the express BET method using SORBI-M instrument with Ar desorption. XRD patterns were recorded on a HZG-4C diffractometer with Cu Kα (35 kV and 35 mA) radiation. The unit cell parameter of the samples and the mean crystallite sizes were estimated from (3 1 1) diffraction line.

Infra-red spectra of the samples (3 mg) pressed with CsI (600 mg) were registered over the 200–4000 cm^{-1} range in transmission mode using a BOMEM MB-102 spectrometer.

The copper dispersion was measured with N_2O decomposition using a high-vacuum static installation. The sample pretreated in an oxygen flow was placed in a quartz reactor then it was evacuated under heating up to 400 °C with 5 °C min^{-1} rate and was kept at this temperature for 40 min in vacuum and for 30 min under 2 Torr O_2 pressure. Further, the sample was degassed and cooled down to 100 °C in vacuum. Then the sample was reduced in H_2 (10 Torr) at 300 °C for 40 min, degassed and cooled to 50 °C under 2 Torr H_2 pressure. The sample was oxidized by nitrous oxide (2 Torr) at 50 °C. The nitrogen formed was analyzed using a mass-spectrometer. The number of the surface copper atoms was calculated from nitrogen formed according to [9]. The copper dispersion was calculated as the ratio between the amount of the surface copper and the total copper content.

Differential dissolution (DD) method was used to determine the phase composition of the catalysts [22]. This method is based on successive dissolution of the sample component phases. The DD analysis was performed in the flow regime at the constant temperature 80 °C and the solvent flow rate 3.5 ml min^{-1}. The solvent concentration and composition were varied in the following order: $H_2O \rightarrow HCl$ (1.2 M) → HF (1:5) and kinetic curves of each element concentration were recorded using an atomic-emission spectrometer with inductively coupled plasma (BAIRD).

The H_2-TPR experiments were carried out in the feed containing 10 vol.% H_2 in Ar. The feed flow rate was 40 ml min^{-1}. The rate of heating from room temperature to 900 °C was 10 °C min^{-1}. During the experiment H_2O was frozen out at −80 °C. The hydrogen concentration was determined using a thermal conductivity detector. For the deconvolution of TPR profiles of the catalysts with alumina and Cr additives, experimental data have been modeled as a superposition of asymmetric Gauss peaks.

XPS data were obtained by a Kratos AXIS 165 spectrometer using monochromatic Al Kα radiation ($h\nu$ = 1486.58 eV) and fixed analyzer pass energy of 40 eV. The binding energy (BE) values referred to the Fermi level were calibrated using the C 1s 284.80 eV, the standard deviation of the peak position associated with the calibration procedure was +0.05 eV.

The catalysts (fraction of 0.25–0.5 mm, volume 0.3–0.4 cm^3) were tested in a U-shaped tubular flow reactor (8 mm i.d.) at atmospheric pressure, GHSV of the reaction mixture (N_2:CH_3OH:-H_2O = 20:40:40 v/v/v) 10,000 h^{-1} and 200–350 °C. Before testing the catalysts were pre-treated at 300 °C for 1 h in the flow of 10 vol.% H_2 in N_2. The stability test of $Cu_{0.2}CZYCr40A$ was carried out at 20,000 GHSV and 300 °C. Two on-line gas chromatographs (GC) "Tsvet-500" equipped with thermal conductivity detectors were used for the analysis of reactants and products. The selectivity of each C-containing product was calculated as a ratio of the product concentration to sum of all C-containing product concentrations.

3. Results and discussion

3.1. Catalyst characterization

3.1.1. BET

The BET specific surface areas (SSA) of the catalysts are listed in Table 1. SSA of the samples ranges from 5 to 33 $m^2\ g^{-1}$ except for $Cu_{0.15}CZ$ with the largest SSA of 72 $m^2\ g^{-1}$. Introduction of yttrium into the samples leads to the decrease in the SSA (compare $Cu_{0.15}C$, $Cu_{0.15}CZ$ and $Cu_{0.15}CZY$). The addition of alumina in the catalyst (>20 wt.%) leads to the increase in SSA from ∼30 to 140 $m^2\ g^{-1}$.

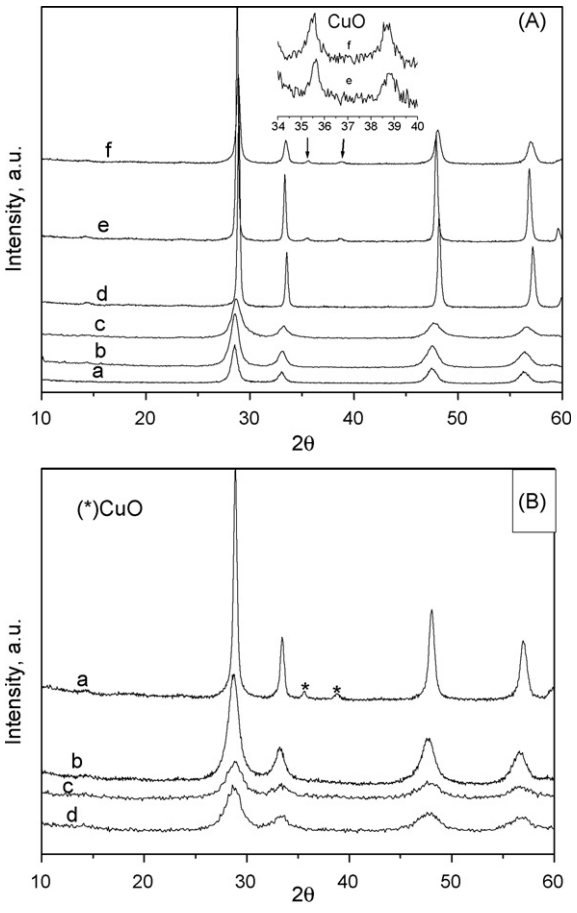

Fig. 1. XRD patterns of the catalysts. A: (a) CeO_2, (b) $Cu_{0.15}C$, (c) $Cu_{0.15}CZ$, (d) CZY, (e) $Cu_{0.15}CZY$ and (f) $Cu_{0.2}CZY$. B: (a) $Cu_{0.2}CZY$, (b) $Cu_{0.2}CZY40A$, (c) $Cu_{0.2}CZYCr40A$ and (d) $Cu_{0.3}CZYCr40A$.

Incorporation of Cr into the catalysts results in a further rise of its SSA up to ~170 $m^2\ g^{-1}$ (Table 1).

The values of copper species dispersion were determined for two samples: $Cu_{0.2}CZY10A$ and $Cu_{0.2}CZYCr40A$. At the same copper concentration (Table 1), the dispersion of copper in $Cu_{0.2}CZY10A$ (14.6%) is noticeably lower compared to $Cu_{0.2}CZYCr40A$ (43%).

3.1.2. XRD and IR spectroscopy

The XRD data are shown in Table 1 and Fig. 1. The cubic solid solution (SS) of *Fd*3*m* fluorite-like structure (JCPDS, No. 43-1002) is present in all samples (Fig. 1). The mean particle sizes of SS are in the range of 10–39 nm and the smallest one (10 nm) is observed in the $Cu_{0.15}CZ$ catalyst. The low-intensity reflections of CuO (JCPDS, No. 44-0706) are observed in the patterns of Cu_xCZY (Fig. 1A). The size of CuO particles calculated from the XRD data increases with the copper content from 10 to 19 nm (Table 1).

For all samples, the diffraction peaks of SS are shifted to higher 2θ as compared with the pure CeO_2 prepared via the urea–nitrate combustion method (Fig. 1) that indicates a contraction of SS lattice (Table 1). The decrease in the SS lattice parameter for $Cu_{0.15}C$ and $Cu_{0.15}CZ$ is due to a smaller ionic radii of Cu^{2+} (0.65 Å) and Zr^{4+} (0.84 Å) than that of Ce^{4+} (0.97 Å), in agreement with [15]. As in the previous studies [15,23], the smaller lattice parameters for CZY and Cu_xCZY are observed despite the larger ionic radius of Y^{3+} (1.019 Å). For Y-doped CeO_2, the contraction of the lattice has been explained using molecular dynamics simulation [24]. The expected effect of the lattice expansion due to substitution of Ce^{4+} by bigger Y^{3+} cations is overcome by the shrinkage of the oxygen sublattice due to shift of oxygen atoms towards the oxygen vacancies. In addition, the introduction of a tri-valent cation in place of Ce^{4+} reduces the Coulomb repulsion force between the nearest cations and makes the M–Ce and M–Y distances shorter. The changes of cation–cation distances may be determined by the balance of the increase of ionic radius (size effect) and the decrease of repulsion force (charge effect). In the case of YDC, the charge effect is larger than the size effect to decrease Y–Ce and Y–Y distances. For our samples, the contraction of Y-doped CeO_2–ZrO_2 solid solution lattice could be due to similar factors.

For the Cu_xCZY samples, the shift of SS reflections toward a lower 2θ value, as compared to that of the CZY oxide without copper (Fig. 1A), indicates the expansion of the lattice (Table 1) due to the difference between the ionic sizes of the Ce^{4+} (0.97 Å) and Ce^{3+}(1.03 Å), which appears in SS [14].

For $Cu_{0.15}C$ and $Cu_{0.15}CZ$, the CuO peaks are absent in the XRD patterns, whereas weak CuO reflections are observed in the XRD patterns of the Cu_xCZY. There are opposite views on the state of copper in the CeO_2-based catalysts including mainly binary Cu–CeO_2 samples or those doped with Zr, Y, La, Sm and other cations [15,16]. The absence of CuO reflections in the catalysts patterns is usually attributed to the incorporation of copper into a solid solution [10,11,25], a fine dispersion of CuO particles on the surface of CeO_2 [13,14,18,26] or a combination of both these factors [27].

The XRD data for the catalysts with alumina and chromium additives are shown in Table 1 and Fig. 1B. As in the samples without additives, the same fluorite-like SS is present in all $Cu_{0.2}CZY(Cr)xA$ samples (Fig. 1B), but the main SS reflections in their XRD patterns are wide. The mean particle size of SS decreases from 16 to 6.3 nm at increasing alumina content from 10 to 40 wt.%. The introduction of chromium leads to a further decreasing of the SS crystallite size to 4.5 nm (Table 1) that corresponds to the high (up to 170 $m^2\ g^{-1}$) SSA of the samples containing alumina and Cr. The copper oxide reflections of a low intensity are observed only in the case of $Cu_{0.2}CZY10A$ sample (Table 1). For all other $Cu_{0.2}CZY(Cr)xA$ catalysts, CuO reflections miss.

Note that in all cases γ-Al_2O_3 phase was not detected by XRD despite of a high (up to 40 wt.%.) alumina content. Two reasons could be responsible for this fact. The first is that in a viscous gel comprising acid nitrates with urea, peptization of γ-Al_2O_3 could occur with a formation of aluminum hydroxide from which the X-ray amorphous alumina is formed after calcination at 400 °C. The second is that alumina and other components interact with

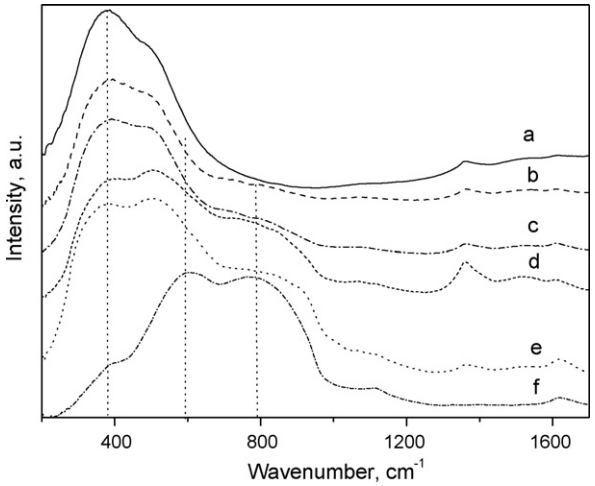

Fig. 2. IR-spectra of the samples: (a) $Cu_{0.2}CZY$, (b) $Cu_{0.2}CZY10A$, (c) $Cu_{0.2}CZY20A$, (d) $Cu_{0.2}CZY40A$, (e) $Cu_{0.2}CZYCr40A$ and (f) Al_2O_3.

formation of a solid solution. To select between these two probable reasons, the catalysts were studied by IR spectroscopy and the DD method as well.

The IR spectra of the catalysts with and without alumina additives and the spectrum of the parent alumina are shown in Fig. 2. For the pure $Cu_{0.2}CZY$ (Fig. 2a), a broad band with a maximum around 370 cm^{-1} and a shoulder near 500 cm^{-1} are present, which is typical for the substituted CeO_2-based SS [28]. In the spectrum of alumina (Fig. 2f), two broad overlapping bands of a high intensity at ~600 and 780 cm^{-1} with a shoulder at ~390 cm^{-1}, as well as low-intensity bands at 1120 and 1620 cm^{-1} are observed, which are characteristic features of γ-Al_2O_3 with a poor crystallinity [28]. In the case of the alumina-containing catalysts (Fig. 2b–e), a broad absorbance in the region of 600–900 cm^{-1} could also be assigned to alumina that is confirmed by the increase in the peak intensity with the alumina concentration. Hence, γ-Al_2O_3 of a poor crystallinity is present in the catalysts. For the alumina and chromium-containing catalysts, the spectra in general are similar but they show a higher absorbance at 700–900 cm^{-1} shifted to the higher frequencies (Fig. 2e). The differential spectra of the catalysts and alumina (not shown for brevity) clarify these peculiarities: the appearance of the band at 928 cm^{-1}, corresponding to Cr–O bond vibration, suggests that the band at 700–900 cm^{-1} is a superposition of the bands assigned to vibrations in alumina and chromia.

3.1.3. Differential dissolution

Differential dissolution method based on consequent dissolution of the sample phases with continuous monitoring of constituting elements concentrations [22] gives additional information on the phase composition and the state of the copper. The presence of different phases, including those invisible for XRD, their exact chemical and quantitative composition, as well as their dispersion could be determined by DD [22]. For $Cu_{0.2}CZY$, the data of DD analysis show that copper along with CuO phase forms two oxide phases of a different composition: Cu–Zr–Ce- and Cu–Ce–Zr–Y-solid solutions of variable composition. The earlier dissolution of the latter phase, as compared to the former one, implies that the Cu–Ce–Zr–Y oxide could be formed at the interface between CuO and Cu–Ce–Zr oxide. These results are in agreement with XPS data (shown below) indicating the enrichment of the catalyst surface with copper. The quantitative analysis of elements testifies that 63% of copper is present as CuO and the rest is incorporated into the solid solution.

The phase composition of the catalysts containing alumina or both alumina and chromium is similar. The catalysts are comprised of yttrium cuprate ($Y_xCu_{1-x}O_3$), Cu–Ce–Zr–Y(Cr) SS of variable composition and alumina, with some admixture of CeO_2 (for $Cu_{0.2}CZY40A$) and Cr_2O_3 as well (for $Cu_{0.2(0.3)}CZYCr40A$). For all catalysts, the main phase is SS of a variable composition and free copper oxide is absent, therefore, all copper is distributed between a solid solution-phase and yttrium cuprate. No data on the aluminum incorporation into SS have been obtained. The kinetics of the phase dissolution allows to consider that finely dispersed $Y_xCu_{1-x}O_3$ species could be located on the surface of Cu–Ce–Zr–Y(Cr) SS particles.

3.1.4. Copper dispersion

The values of copper species dispersion were determined for two selected samples. At the same concentration (Table 1), the copper dispersion was 14.6% and 43% for $Cu_{0.2}CZY10A$ and $Cu_{0.2}CZYCr40A$, correspondingly. Hence, the increase of Al_2O_3 content and addition of Cr provide for the formation of highly dispersed copper species. Additionally, for $Cu_{0.2}CZYCr40A$, in situ XRD data were obtained during the sample reduction in the hydrogen feed at 300 °C. The XRD pattern of the initial oxidized sample does not show CuO reflections and the reflections of metallic copper was found to be absent in the pattern of the reduced sample that confirms the presence of highly dispersed copper species. In the case of an oxidized $Cu_{0.2}CZY10A$ sample which contains 10% of alumina, the copper oxide reflections (Table 1) of a low intensity are observed in XRD pattern (not present in the paper) that is in agreement with the low (14.6%) copper dispersion.

Table 2
XPS data on the surface composition of the catalysts

Catalyst	Cu/Ce		Y/Ce	
	Vol.	Surf.	Vol.	Surf.
$Cu_{0.2}CZY$	0.46	0.78	0.16	1.14
$Cu_{0.2}CZY40A$	0.39	0.92	0.15	1.21
$Cu_{0.2}CZYCr40A$	0.42	0.58	0.12	0.60

3.1.5. XPS

For $Cu_{0.2}CZY$, $Cu_{0.2}CZY40A$ and $Cu_{0.2}CZYCr40A$, the chemical composition of the catalyst surface is studied by XPS. The surface and bulk concentration ratio of Cu/Ce and Y/Ce are presented in Table 2. The higher values of the surface ratio evidence the copper and yttrium segregation on the catalyst surface. The smaller enrichment of the surface with copper and yttrium is observed for the $Cu_{0.2}CZYCr40A$ sample.

3.2. Temperature-programmed reduction by hydrogen

H_2-TPR profiles of CeO_2 and CZY, and Cu-containing catalysts without alumina and Cr are shown in Fig. 3. The spectrum of CeO_2 shows overlapping peaks at ~400 and 500 °C and a peak at ~820 °C corresponding to reduction of some mobile oxygen forms and the lattice oxygen of CeO_2, respectively [29,30]. Meanwhile, the CZY sample shows one broad peak at 600 °C. Such a profile with a shift to lower temperature suggests the weakening of Ce(Zr,Y)–O bonds in the lattice of SS caused by incorporation of the dopant [31].

For Cu-containing catalysts, an intensive peak with maximum at 180–205 °C and a broad peak of a low intensity at a high temperature (Fig. 3) are observed. The low-temperature peak could be attributed mainly to the reduction of copper species, whereas the high-temperature peak is related to the reduction of Ce^{4+} [11,32,33]. For the catalysts without Al_2O_3 and Cr, the position

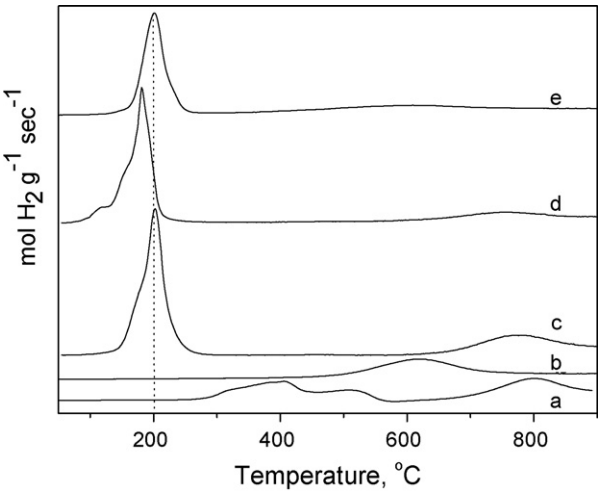

Fig. 3. H_2-TPR spectra of the catalysts without additives: (a) CeO_2, (b) CZY, (c) $Cu_{0.15}C$, (d) $Cu_{0.15}CZ$ and (e) $Cu_{0.15}CZY$.

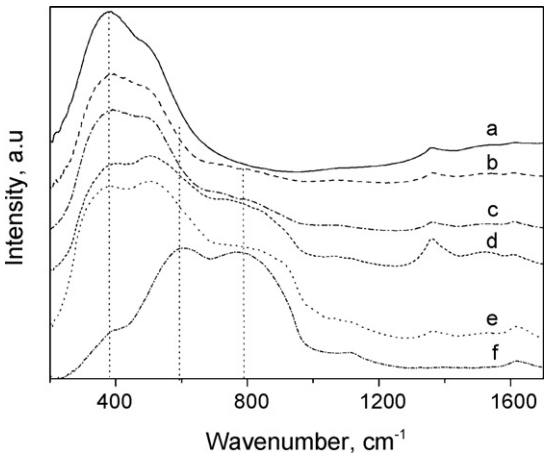

Fig. 4. H_2-TPR spectra of (a) $Cu_{0.2}CZY$, (b) $Cu_{0.2}CZY10A$, (c) $Cu_{0.2}CZY20A$, (d) $Cu_{0.2}CZY40A$, (e) $Cu_{0.2}CZYCr40A$ and (f) $Cu_{0.3}CZYCr40A$.

and the profile of the peaks depend on the dopants. The introduction of Zr into the Cu–CeO_2 (sample $Cu_{0.15}CZ$) leads to the shift of both peaks to lower temperatures and the appearance of low-temperature shoulders for the peak at 180 °C (Fig. 3d). Addition of both Zr and Y results in the more symmetrical profile of the low-temperature peak at 200 °C (Fig. 3e), while the high-temperature peak is shifted to lower temperature and is situated at 600 °C as for CZY (Fig. 3b).

In the case of the catalysts containing Al_2O_3 and chromium additives, the main features of the spectra are the same: a low temperature overlapping peak below 350 °C and a high-temperature broad peak (not shown) are present (Fig. 4). It is known that the TPR profiles of Cu–CeO_2-based catalysts are quite sensitive on the method of their preparation [14], chemical composition [15], concentration of Cu [11]. However, in all cases several peaks in the low-temperature region are observed which are attributed to copper oxide species with a different dispersion. The temperature of their reduction increases in the order: highly dispersed CuO clusters in a close contact with CeO_2 < isolated Cu^{2+} cations and small two- and three-dimensional clusters < large three-dimensional clusters and bulk CuO [29,30,32–35]. Therefore, the noticeable broadening of the low-temperature peak could evidence that, in these catalysts, dispersion of oxide copper species strongly varies whereas its shift to a low-temperature region observed at increasing Al_2O_3 content and Cr addition could be attributed to formation of highly dispersed copper species. Indeed, for $Cu_{0.2}CZYCr40A$, the copper dispersion is 43% that is significantly higher as compared to $Cu_{0.2}CZY10A$ (14.6%).

In order to separate the features of the low-temperature peak (Fig. 4) we have carried out a deconvolution of the TPR peak profiles. The derived peaks were sorted in three groups by the temperature of their maximum: below 190 °C, in the range of 210–270 °C and above 630 °C (Table 3). At increasing Al_2O_3 loading, the amount of hydrogen consumed in the peak with the maximum below 190 °C increases from 4% ($Cu_{0.2}CZY$) to 14–15% ($Cu_{0.2}CZY$(-Cr)40A), while hydrogen consumption in the peak with the maximum above 630 °C decreases from 14 to 1–2%, correspondingly (Table 3). The average value of hydrogen consumption in the peaks at 210–270 °C changes insignificantly being about 83%. Note, that for the $Cu_{0.2}CZY(Cr)yA$ catalysts with a high SSA, UV–vis data (not shown here) evidence mainly the presence of isolated Cu^{2+} ions and their clusters that is conditioned by the formation of surface $CuYO_x$ species and incorporation of all remaining Cu into SS as DD data show. Thus, the increase of hydrogen consumption in the derived peak with maximum below 190 °C could be caused by reduction of such highly dispersed species.

Table 3
Hydrogen consumption in the peaks derived by deconvolution of H_2-TPR profiles for the catalysts with Al_2O_3 and Cr additives

Catalyst	H_2 consumption (%)		
	<190 °C	210–270 °C	>630 °C
$Cu_{0.2}CZY$	4	82	14
$Cu_{0.2}CZY10A$	7	83	10
$Cu_{0.2}CZY20A$	13	78	9
$Cu_{0.2}CZY40A$	15	83	2
$Cu_{0.2}CZYCr40A$	14	82	4
$Cu_{0.3}CZYCr40A$	14	85	1

Peaks are grouped by the temperature of their maximum.

Furthermore, the decrease of H_2 consumption in the high-temperature peak and simultaneous increase of its consumption at low temperatures imply that at temperature below 400 °C both the surface and bulk reduction of the samples could occur that was also shown for $Ce_{1-x}Cu_xO_y$ solid solutions [10–14]. Indeed, for all catalysts, the ratio of the total H_2 consumption in the low-temperature peak (at 30–400 °C) to Cu concentration is above one. This means, that at this relatively low-temperature partial reduction of Ce^{4+} occurs simultaneously with the reduction of copper cations [10,11,32,33]. It is believed that reduction of Ce^{4+} at relatively low temperatures evidences the increase of the lattice oxygen mobility in SS.

The position of the low-temperature peak was shown to depend on the dispersion of oxidized copper particles, shifting to low temperatures with the dispersion increase [32,36]. The area of corresponding peak is apparently proportional to the amount of copper and cerium in the sample, while its height is determined by the maximum oxygen flux from the bulk of particles to their surface which can be achieved for a given sample composition in a given temperature range. Since the oxygen flux is controlled by the lattice oxygen mobility, this suggests that the maximum rate of reduction at a close Cu and Ce content in the same temperature range can be used as an approximate measure of the lattice oxygen mobility. This conclusion was verified in the case of ceria and ceria-zirconia solid solutions doped with Zr, La, Pr, Gd by directly comparing maximum rates of samples reduction by H_2 with the lattice oxygen mobility estimated by oxygen isotope hetero-exchange [31].

3.3. Catalytic activity in steam reforming of methanol

The temperature dependence of methanol conversion and CO_2 selectivity for the catalysts without alumina and Cr are shown in Fig. 5. For all samples, methanol conversion increases with the temperature. At the same Cu content (Table 1), introduction of Zr into Cu/CeO_2 system results in a higher conversion (Fig. 5A, compare $Cu_{0.15}C$ and $Cu_{0.15}CZ$). When Y and Zr are added ($Cu_{0.15}CZY$), some conversion decrease is observed as compared to $Cu_{0.15}C$. Such changes of the conversion are mainly determined by the SSA of the samples depending on their composition (Table 1). Though $Cu_{0.15}CZ$ with the highest SSA shows the highest conversion of methanol its CO_2 selectivity is the lowest (Fig. 5B). The highest selectivity is revealed for the $Cu_{0.15}CZY$ sample.

For Cu_xCZY catalysts, the rate of hydrogen production increases with the copper concentration (Fig. 5A). Note, that CO_2 selectivity over Cu_xCZY catalysts is 100% at 250–300 °C and decreases to 97.7–98.9% at 350 °C. CO is the main by-product appearing only at 350 °C though this is possible by thermodynamics at much lower temperatures. These results indicate that reaction sequence is such that CO_2 and H_2 are the primary products of the reaction and that CO is formed at higher temperatures by the reverse water-gas

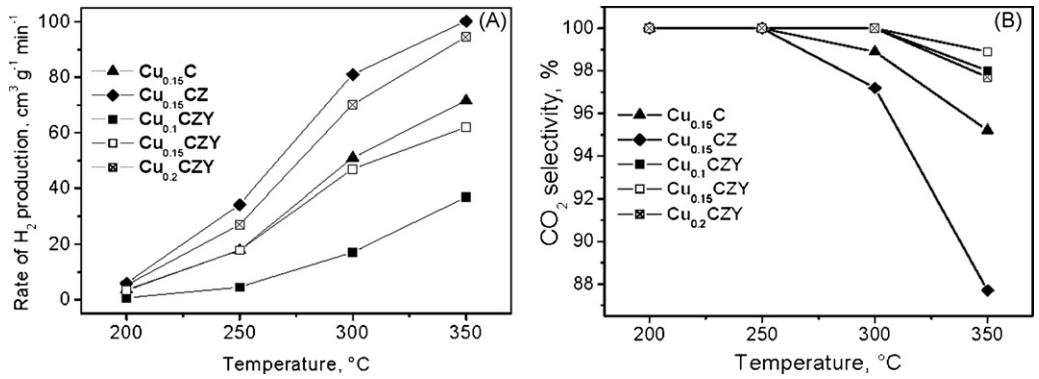

Fig. 5. (A) Methanol conversion and (B) CO_2 selectivity, in SRM over the catalysts without additivies.

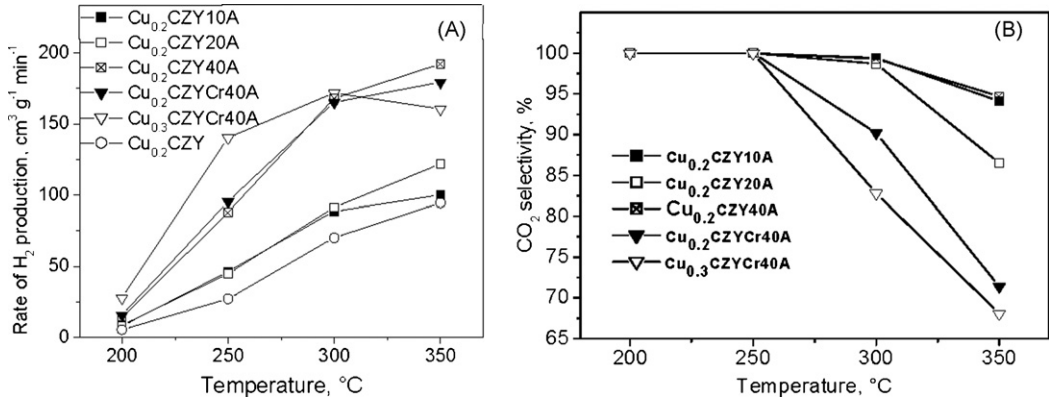

Fig. 6. (A) Rate of H_2 production and (B) CO_2 selectivity, in SRM over the catalysts with alumina and chromium.

shift reaction (RWGS). Similar results were obtained by Breen and Ross [7] for various Cu–Zn-based catalysts.

The hydrogen production rate and CO_2 selectivity in SRM over $Cu_{0.2}CZY(Cr)xA$ catalysts are shown in Fig. 6. Addition of Al_2O_3 and Cr results in the increase of the H_2 production rate depending on the alumina content (Fig. 6A). Introduction of 10–20 wt.% Al_2O_3 results in a minor increase of the H_2 production rate with close values being determined for $Cu_{0.2}CZY10A$ and $Cu_{0.2}CZY20A$ samples. The increase of Al_2O_3 content up to 40% leads to the pronounced rise of H_2 production rate (Fig. 6A, $Cu_{0.2}CZY40A$). This could be related to the increase of the copper dispersion with the addition of Al_2O_3. Indeed, the copper dispersion was 14.6% and 43% for $Cu_{0.2}CZY10A$ and $Cu_{0.2}CZYCr40A$, correspondingly.

At the same copper concentration, addition of Cr does not affect the rate (Fig. 6A, $Cu_{0.2}CZYCr40A$), while the simultaneous increase of the copper concentration favours its noticeable rise at 250 °C (Fig. 6A, $Cu_{0.3}CZYCr40A$). Furthermore, when for $Cu_{0.2}CZYCr40A$ and $Cu_{0.2}CZY40A$, the rate of H_2 production increases with the temperature, for $Cu_{0.3}CZY(Cr)40A$ it goes through a maximum at 300 °C. Note, that for two former catalysts, at 300 °C, a bend in the temperature dependence of the hydrogen production rate is observed. Such a decrease of the hydrogen production rate can be explained by increasing contribution of RWGS into the overall reaction rate at temperatures above 300 °C.

As compared with the pure $Cu_{0.2}CZY$ catalyst, addition of alumina and chromium leads to the decrease of selectivity to CO_2 at temperatures above 250 °C (Fig. 6B), and along with the main by-product—CO, the traces of dimethyl ether appear. This is caused by a high acidity of alumina and chromia revealed in the catalysts by IR and DD which favour occurring of methanol dehydration [3]. Chromia decreases CO_2 selectivity in substantially greater extent than alumina, which can be assigned to its higher acidity. Decline of CO_2 selectivity could be also a result of RWGS reaction. Nevertheless, concentration of CO is lower as compared with calculated equilibrium values even at 350 °C (Fig. 7).

Study of the catalysts stability at 350 °C (Fig. 8) showed that pure $Cu_{0.2}CZY$ rapidly loses its activity. The addition of 40 wt.% alumina significantly increases the catalyst stability, though it is still slowly reduced with the time-on-steam. The $Cu_{0.2}CZYCr40A$ catalyst does not lose any activity at all demonstrating 100% methanol conversion during the experiment. For the activity change to be visible this catalyst was tested at 20,000 GHSV and 300 °C during 17 h (Fig. 9). The results show that the catalyst is sufficiently effective and stable at such high GHSV. It is believed

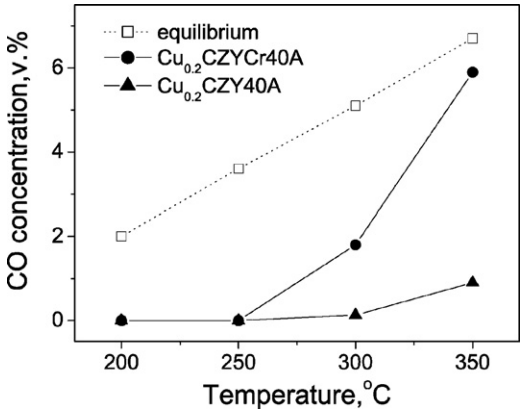

Fig. 7. Calculated and experimental CO concentration over $Cu_{0.2}CZY40A$ and $Cu_{0.2}CZYCr40A$.

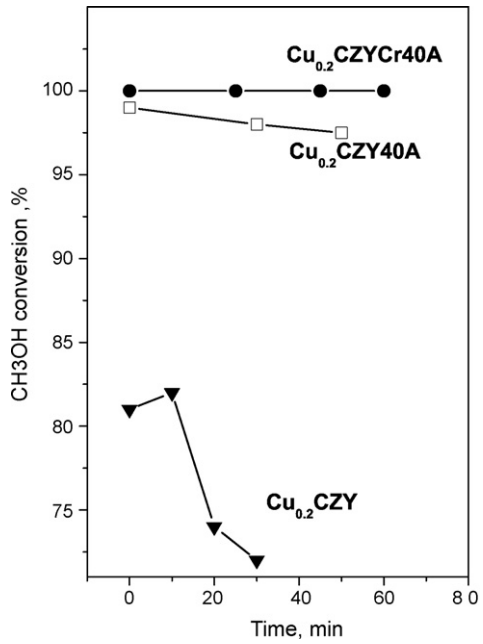

Fig. 8. Influence of the catalyst composition on methanol conversion in SR at 350 °C.

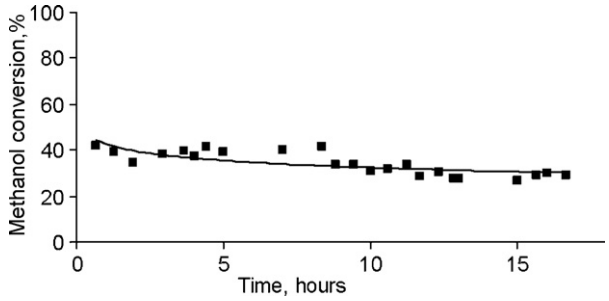

Fig. 9. Time dependence of methanol conversion over $Cu_{0.2}CZYCr40A$ at 300 °C and 20,000 GHSV.

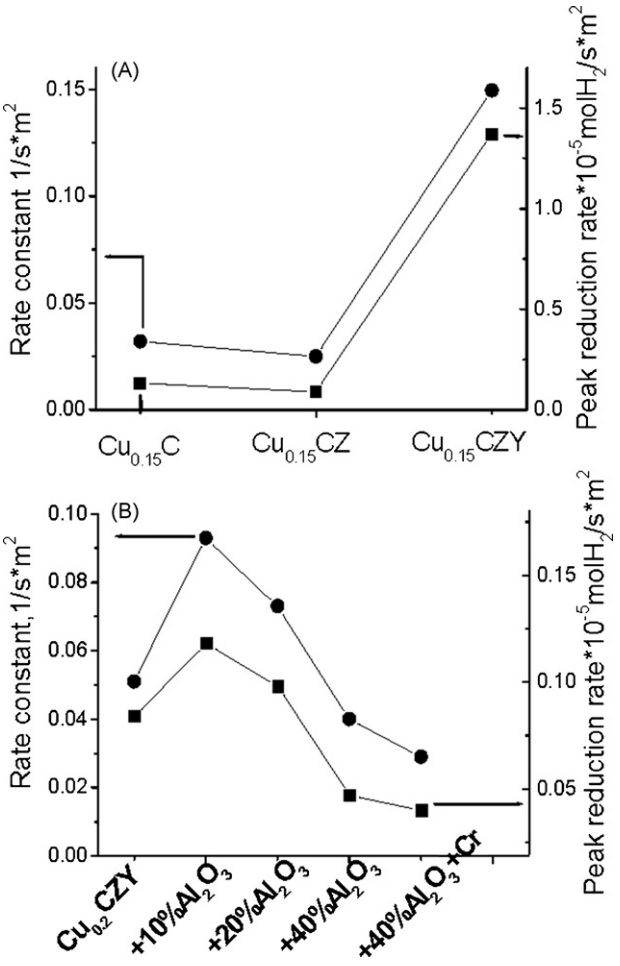

Fig. 10. Correlation in the reaction rate constant and peak rate of reduction during H_2-TPR. (A) $Cu_{0.15}C$, $Cu_{0.15}CZ$, $Cu_{0.15}CZY$ and (B) $Cu_{0.2}CZY$, $Cu_{0.2}CZY10A$, $Cu_{0.2}CZY20A$, $Cu_{0.2}CZY40A$, $Cu_{0.2}CZYCr40A$ catalysts.

that while alumina helps to disperse active copper species, chromium could act as a textural promoter of copper preventing it's sintering [19,20].

3.4. Correlation of SRM specific rate constant and solid solution oxygen mobility

For the Pt catalysts based on doped CeO_2 and CeO_2–ZrO_2, along with influence of Pt dispersion on the catalytic activity in the reaction of methane selective oxidation into syngas, strong parallelism is observed between parameters characterizing their lattice oxygen mobility (peak rates of H_2-TPR) and specific reaction rates [36]. Taking into account H_2-TPR data of this work (Figs. 3 and 4), we compare the maximal rates of the catalyst reduction with hydrogen and the rate constants of the SRM reaction related per the total surface unit of the samples. The correlation between these values for the samples with and without alumina and Cr is shown in Fig. 10. It could be clearly seen the parallel change of peak reduction rates and SRM reaction rate constants at variation of the oxide composition. For the samples without alumina and Cr (Fig. 10A), the maximal rate of reduction decreases when irreducible zirconium is introduced into copper-doped ceria evidencing the decrease of lattice oxygen mobility. This is reflected in decreasing the rate constant of methanol steam reforming reaction. Incorporation of triple-charged yttrium cations into fluorite-like oxide lattice leading to generation of anion vacancies increases the oxygen mobility and the reaction rate constant of SRM.

The same correlation is observed for the catalysts with addition of alumina and chromium (Fig. 10B). Addition of 10 wt.% of alumina does not change SSA (Table 1) but leads to the increase of the peak reduction rate. This fact evidences the increase of oxygen mobility probably due to generation of extended defects (domain boundaries, etc.) as can be inferred from a decline of X-ray particle size (domain size) (Table 1). At increasing alumina concentration the peak rate of reduction and rate constant decrease. This is probably explained by the decoration of copper with dispersed alumina particles revealed by IR data. As a result of such a decoration, the oxygen transfer from the bulk of solid solution to copper species could be hampered, thus decreasing the peak rate of reduction. The parallel decrease of a SRM rate constant was suggested to be due to the block of the lattice oxygen transfer to copper that retards transformation of reaction intermediates into desired products and prevent the formation of oxygenated polymers—coke precursors. In other words, the mobility of lattice oxygen is an important factor for steam reforming of methanol.

4. Conclusions

The hydrogen production rate and selectivity in SRM of catalysts prepared using urea–nitrate combustion method

($Cu_xCe_{1-x}O_y$, pure and promoted by Zr or both Zr and Y, and $Cu_x(CeZrY)_{1-x}O_y$ with addition of alumina and chromium) were shown to depend on their composition. Doping of $Cu_xCe_{1-x}O_y$ with Zr results in the increase of the methanol conversion and hydrogen production rate due to a high SSA, while CO_2 selectivity decreases. Incorporation of both Zr and Y slightly influences the methanol conversion and hydrogen production rate and increases CO_2 selectivity up to 100% at 300 °C. For $Cu_x(CeZrY)_{1-x}O_y$ catalysts, in which copper is distributed between the solid solution and CuO phase according to XRD and DD methods, methanol conversion and H_2 production rate rises with increasing copper concentration. Addition of alumina and chromia to $Cu_x(CeZrY)_{1-x}O_y$ leads to a significant increase of the hydrogen production rate due to a high SSA (up to 170 $m^2 g^{-1}$) and appearance of highly dispersed copper species. Above 300 °C, CO_2 selectivity of Al_2O_3 and Cr-containing catalysts is lower as compared to pure $Cu_x(CeZrY)_{1-x}O_y$, however, their stability is higher. It is suggested that alumina helps to disperse active copper species and chromium acts as a textural promoter of copper preventing it sintering.

Comparison of SRM specific rate constants and maximal rates of reduction with hydrogen characterizing mobility of catalyst lattice oxygen shows their parallel change at variation of the catalyst composition. Therefore, the efficient transfer of lattice oxygen to copper clusters could facilitate transformation of reaction intermediates into desired products and prevent the formation of oxygenated polymers precursors of coke. In other words, the mobility of lattice oxygen is an important factor for steam reforming of methanol.

Acknowledgements

The authors gratefully acknowledge the financial support from INTAS (05-1000005-7663 project) and Dr. E. Starokon for measuring copper dispersion.

References

[1] I. Ritzkopf, S. Vukojevic, C. Weidenthaler, J.-D. Grunwaldt, F. Schuth, Appl. Catal. A: Gen. 302 (2006) 215.
[2] C. Song, Catal. Today 77 (2002) 17.
[3] J. Agrell, B. Lindstrom, L.J. Pettersson, S.G. Jaras, in: J.J. Spivey (Ed.), Catalysis—Specialist Periodical Reports, vol. 16, 2002, p. 67.
[4] D.L. Trimm, Z.I. Onsan, Catal. Rev. 43 (2001) 31.
[5] Y.-M. Lin, M.-H. Rei, Catal. Today 67 (2001) 77.
[6] M.P. Harold, B. Nair, G. Kolios, Chem. Eng. Sci. 58 (2003) 2551.
[7] J.P. Breen, J.R.H. Ross, Catal. Today 51 (1999) 521.
[8] S. Velu, K. Suzuki, Top. Catal. 22 (2003) 235.
[9] A. Mastalir, B. Frank, A. Szizybalski, H. Soerijanto, A. Deshpande, M. Niederberger, R. Schomäcker, R. Schlögl, T. Ressler, J. Catal. 230 (2005) 464.
[10] Y. Liu, T. Hayakawa, K. Suzuki, S. Hamakawa, Catal. Commun. 2 (2001) 195.
[11] Y. Liu, T. Hayakawa, K. Suzuki, S. Hamakawa, T. Tsunoda, T. Ishii, M. Kumagai, Appl. Catal. A 223 (2002) 137.
[12] X. Zhang, P. Shi, J. Mol. Catal. A: Chem. 194 (2003) 99.
[13] J. Papavasiliou, G. Avgouropoulos, T. Ionnides, Catal. Commun. 5 (2004) 231.
[14] W. Shan, Z. Feng, Z. Li, J. Zhang, W. Shen, C. Li, J. Catal. 226 (2004) 206.
[15] J. Papavasiliou, G. Avgouropoulos, T. Ioannides, Appl. Catal. B: Environ. 69 (2006) 226.
[16] H. Oguchi, T. Nishiguchi, T. Matsumoto, H. Kanai, K. Utani, Y. Matsumura, S. Imamura, Appl. Catal. A 281 (2005) 69.
[17] W.-H. Cheng, I. Chen, J.-S. Liou, S.-S. Lin, Topics Catal. 22 (2003) 225.
[18] H. He, H.X. Dai, C.T. Au, Catal. Today 90 (2004) 245.
[19] Z. Wang, J. Xi, W. Wang, G. Lu, J. Mol. Catal. A: Chem. 191 (2003) 123.
[20] N.A.S. Amin, E.F. Tan, Z.A. Manan, J. Catal. 222 (2004) 100.
[21] J.B. Wang, H.-K. Lee, T.-J. Huang, Catal. Lett. 83 (2002) 79.
[22] V.V. Malakhov, J. Mol. Catal. A: Chem. 158 (2000) 143.
[23] W.-P. Dow, Y. Piao, T.-J. Huang, Appl. Catal. A: G 190 (2000) 25–34.
[24] H. Hayashi, R. Sagawa, H. Inaba, K. Kawamura, Solid State Ionics 131 (2000) 281.
[25] C. Lamonier, A. Ponchel, A. D'Huysser, L. Jalowiecki-Duhamel, Catal. Today 50 (1999) 247.
[26] Lj. Kundakovic, M. Flytzani-Stephanopoulos, Appl. Catal. A 171 (1998) 13.
[27] S. Hoscvar, U.O. Krasovec, B. Orel, A.S. Aricy, H. Kim, Appl. Catal. B 28 (2000) 113.
[28] A. Boldyrev, IR Spectra of Minerals, Nedra, Moscow, 1976.
[29] M. Manzoli, R.D. Monte, F. Boccuzzi, S. Coluccia, J. Kaspar, Appl. Catal. B 61 (2005) 192.
[30] G. Avgouropoulos, T. Ioannides, Appl. Catal. B 67 (2006) 1.
[31] V.A. Sadykov, N.V. Mezentseva, G.M. Alikina, et al. Solid State Phenomena 128 (2007) 239.
[32] P. Zimmer, A. Tschope, R. Birringer, J. Catal. 205 (2002) 339.
[33] X. Tang, B. Zhang, Y. Li, Y. Xu, Q. Xin, W. Shen, Catal. Today 93–95 (2004) 191.
[34] G. Avgouropoulos, T. Ioannides, Appl. Catal. A 244 (2003) 155.
[35] E. Moretti, M. Lenarda, L. Storaro, A. Talon, R. Frattini, S. Polizzi, E. Rodriguez-Castellon, A. Jimenez-Lopez, Appl. Catal. B 72 (2006) 149.
[36] V.A. Sadykov, T.G. Kuznetsova, et al. Catal. Today 117 (2006) 475.